

RI 9427

REPORT OF INVESTIGATIONS/1992

Large-Scale Strata Response to Longwall Mining: A Case Study

By R. O. Kneisley and K. Y. Haramy

UNITED STATES DEPARTMENT OF THE INTERIOR



BUREAU OF MINES



Report of Investigations 9427

Large-Scale Strata Response to Longwall Mining: A Case Study

By R. O. Kneisley and K. Y. Haramy

**UNITED STATES DEPARTMENT OF THE INTERIOR
Manuel Lujan, Jr., Secretary**

**BUREAU OF MINES
T S Ary, Director**

Library of Congress Cataloging in Publication Data:

Kneisley, R. O. (Richard O.)

Large-scale strata response to longwall mining : a case study / by R.O. Kneisley and K.Y. Haramy.

p. cm. — (Report of investigations / Bureau of Mines; 9427)

Includes bibliographical references (p. 24).

1. Rock mechanics—Colorado—Steamboat Springs Region. 2. Longwall mining—Colorado—Steamboat Springs Region. 3. Time-domain analysis. I. Haramy, Khamis Y. II. Title. III. Series: Report of investigations (United States. Bureau of Mines); 9427.

TN23.U43 [TN317] 622 s—dc20 [622'.334] 92-10295 CIP

CONTENTS

| | <i>Page</i> |
|--|-------------|
| Abstract | 1 |
| Introduction | 2 |
| Mine description | 2 |
| Generalized stratigraphy, structure, and stress fields | 2 |
| Site geology and physical properties | 4 |
| Data analysis | 6 |
| Main roof caving action | 6 |
| Pressure measurements | 13 |
| Forward abutment studies | 13 |
| Yield pillar behavior | 15 |
| Load transfer mechanisms | 19 |
| Summary and conclusions | 24 |
| References | 24 |

ILLUSTRATIONS

| | |
|---|----|
| 1. Generalized stratigraphic column | 3 |
| 2. Geologic structure and in situ stress fields | 3 |
| 3. Mine layout and study site locations | 5 |
| 4. Instrumentation location detail of panel 1 | 5 |
| 5. Stratigraphic column of headgate sites of middle-entry roofs | 6 |
| 6. Instrumentation detail of site H | 7 |
| 7. Instrumentation detail of site B | 8 |
| 8. Instrumentation detail of site T | 9 |
| 9. Instrumentation detail of site A | 10 |
| 10. Typical TDR survey with tensile roof break | 11 |
| 11. Main roof caving of panel 1 versus face distance and time | 11 |
| 12. Suggested sequence of main roof caving | 12 |
| 13. Subsidence development versus face distance and time | 13 |
| 14. Forward abutment pressure at headgate site H | 14 |
| 15. Forward abutment pressure at tailgate site T | 14 |
| 16. Forward abutment pressure at headgate site B | 15 |
| 17. Stress profiles of panel rib at 0-ft face distance | 15 |
| 18. Forward abutment pressure of stress site at site T | 15 |
| 19. Stress state from cell readings at 0-ft face distance | 16 |
| 20. Vertical pressure readings in yield pillars | 17 |
| 21. Comparison of estimated yield pillar width, Wilson versus Karmis-Chen approach | 18 |
| 22. Stress profiles at headgate site H | 19 |
| 23. Stress profiles at headgate site B | 21 |
| 24. Mean pressure increases at headgate sites H and B | 22 |
| 25. Panel 1 mining effect on tailgate and headgate pressure distribution at sites T and H | 23 |
| 26. Panel 1 mining effect on tailgate and headgate pressure distribution at sites A and B | 23 |

TABLES

| | |
|---|---|
| 1. Summary of physical properties tests | 4 |
| 2. Summary of tensile strength tests | 4 |

UNIT OF MEASURE ABBREVIATIONS USED IN THIS REPORT

deg degree

ft foot

in inch

m meter

pci pound (force) per cubic inch

pct percent

psi pound (force) per square inch

ton/ft² ton per square foot

LARGE-SCALE STRATA RESPONSE TO LONGWALL MINING: A CASE STUDY

By R. O. Kneisley¹ and K. Y. Haramy²

ABSTRACT

This U.S. Bureau of Mines report summarizes a study of large-scale strata response to longwall mining at a western U.S. coal mine. This study utilized surface and subsurface measurements, geologic mapping, in situ stress measurements, and pressure cell readings to characterize strata behavior. Preliminary analysis of surface subsidence and time-domain reflectometry (TDR) was used to determine a suggested main roof caving sequence. Coal ejected from the face apparently resulted from brittle failures that occurred because of lack of significant yield zone development. The combination of a strong coal with pronounced directional behavior, low overburden pressures, a good caving roof, and a high-production environment that minimized time-dependent loading apparently reduced yielding of the longwall face. The panel 1 headgate-entry design appears adequate; however, the abutment pillar and adjacent panel tailgate rib are highly stressed and may contribute to problems during second panel mining. The small chain pillar yielded after passage of the face, but the pillar width may be near maximum since evidence of a stressed core exists.

¹Mining engineer.

²Supervisory mining engineer.

Denver Research Center, U.S. Bureau of Mines, Denver, CO.

INTRODUCTION

A geotechnical study was conducted at a western U.S. coal mine to assess large-scale strata response during the extraction of the initial longwall panel. This study included surface and subsurface studies in conjunction with an in-mine demonstration of an automated, mine-wide ground control monitoring system. Details regarding the installation and operation of the monitoring system are presented in reports by Hanna, Conover, and Haramy (1-3).³

Surface subsidence and subsurface measurements to characterize main roof caving and pressure measurements to describe pillar and panel response to longwall mining were used in the geotechnical investigations. Of special concern were caving of the mine roof, since both the immediate and main roof contained competent sandstone units, and the in-mine behavior of the headgate chain

pillars. The three-entry headgate system included one yield pillar, adjacent to the active panel and designed to yield with first panel mining, and a larger abutment pillar, sized to support mining-induced panel 1 loading yet yield with second panel mining. The headgate chain pillars were designed not only to provide support during mining of the Wadge Seam but also, through controlled yielding and resultant load transfer, to reduce potential stress-induced problems in the subadjacent Wolf Creek Seams, approximately 135 ft below the active seam and tentatively planned for future mining (4).

This study was begun prior to the startup of panel 1; ground control measurements have been monitored since mining commenced.

MINE DESCRIPTION

The mine, located approximately 20 miles southwest of Steamboat Springs, CO, was opened in 1983 and, following a 1988 decision, converted from room-and-pillar to longwall mining. The first panel, under approximately 1,050 ft of cover, was developed in the lowest portion of the mine to facilitate drainage and pumping of ground water to the surface. Panel 1, approximately 620 ft wide by 7,200 ft long, retreated from west to east and was oriented at approximately 45° to the major and minor joint sets to facilitate roof caving (4).

Panel 1 included three-entry gate roads. The panel 1 tailgate utilized 80-ft-square pillars on 100-ft centers; the headgate used a 35-ft-wide yield pillar and an 80-ft-wide abutment pillar, both 80 ft long. The headgate chain pillars were sized to increase coal recovery, to provide first and second panel mining entry stability, and to minimize stress concentrations in the subadjacent Wolf Creek Seams.

GENERALIZED STRATIGRAPHY, STRUCTURE, AND STRESS FIELDS

The mine is located on the south flank of a structural basin, the southeastern most extension of the Washakie-Sand Wash Basin of northwestern Colorado and south-central Wyoming. The coal measures approximately 300 ft thick, occurs in the Mount Harris Member of the Upper Cretaceous Williams Fork Formation, and is bounded by two massive sandstone beds: the Trout Creek and the Twentymile (fig. 1). The coalbed being mined, the Wadge Seam, is 8.5 to 10 ft thick. The immediate roof consists primarily of mudstone and sandstone sequences. Of particular interest, because of potential roof caving problems, is an up to 25-ft-thick sandstone bed, approximately 12 to 15 ft above the coalbed. The immediate floor consists of bone coal, carbonaceous mudstones, channel sandstones,

and thin coals (4). The Wolf Creek Seams (135 ft below) are being considered for future mining.

The geologic structure underwent two deformational periods. The first period produced predominantly large north-trending folds and associated strike-slip and reverse faults. The second period produced generally northwest-striking normal faults (fig. 2). Structurally, the seam is regular, strikes N. 50° E., and dips N. 7° W., except near the Oak Creek anticline where the strike is N. 70° E. and the dip is 8° to the north. The topography parallels the dip, and the overburden is constant over the longwall area, 1,060 to 1,100 ft thick. The seam exhibits prominent cleating; the face cleat is consistently oriented N. 45° to 70° W. and dips both southwest and northeast. The less well-defined butt cleat roughly parallels the secondary roof joint set, striking at N. 40° to 60° E. The major joint system strikes at N. 35° to 70° W., with one set dipping at 65° to

³Italic numbers in parentheses refer to items in the list of references at the end of this report.

85° SW. and the complementary set dipping at 80° to 90° SE. (4). The in situ field was determined using the overcoring technique (4-5). Figure 2 shows the test locations and the magnitude and direction of the maximum and minimum secondary stresses. Measurements from tests performed in the main entries and closer to the portal indicated the existence of excessive horizontal stress; that is, stress levels exceeding values expected from Poisson's effect. Subsequently, the entries were developed at approximately 45° to both the geologic structure and to the major principal stress direction (4). While these earlier test results indicated a generally northwest-trending stress direction, two test sets performed closer to panel 1 show a nearly east-west stress direction. Whether this apparent rotation of stress direction is due to influence of the fault zone, more accurately represents the panel 1 stress state, or results from other factors is unknown. Maleki (4) suggests that the mine roof stress distribution is controlled more by bed thickness than by elastic modulus. Possible slippage along slickensided mudstone-sandstone interfaces moderates stresses in the weaker roof zones and subsequently concentrates stresses in the more intact roof zones. The resulting stress redistribution is thought to contribute to minor cutter roof at the pillar corners (4).

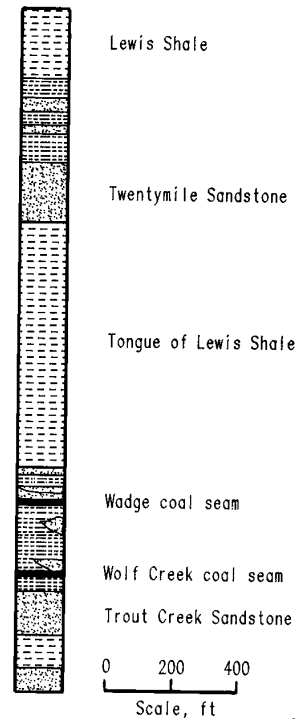


Figure 1.—Generalized stratigraphic column.

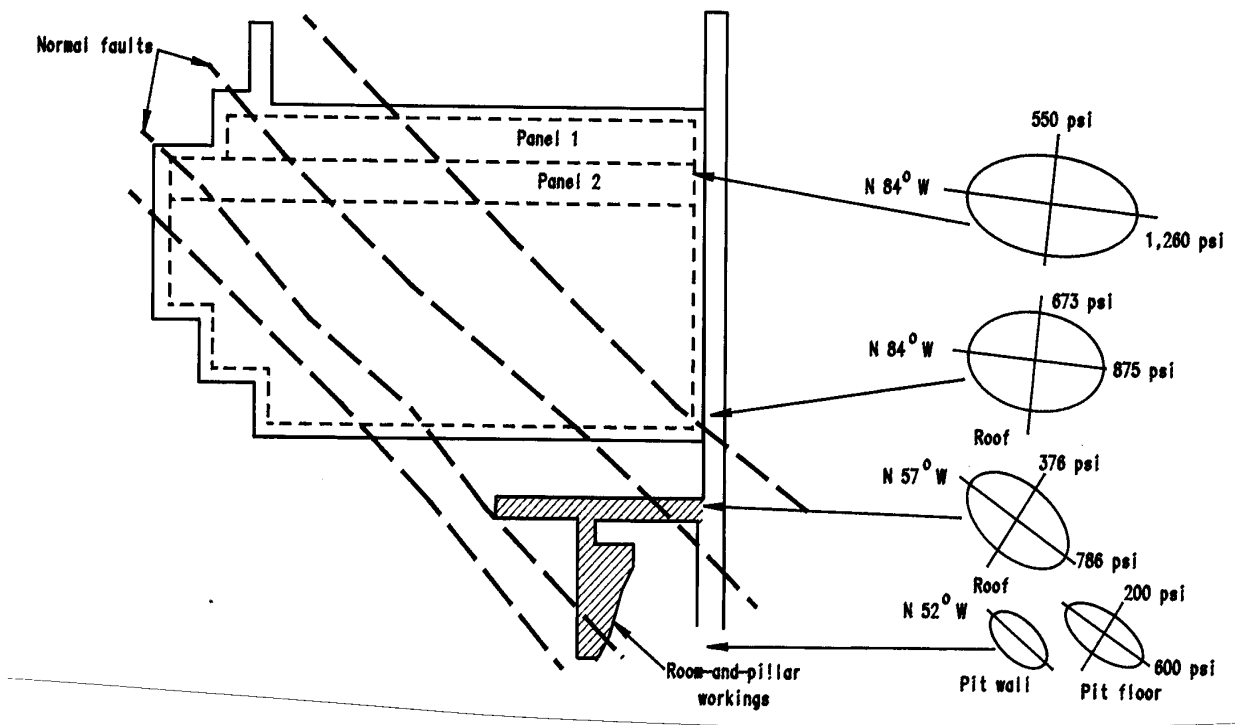


Figure 2.—Geologic structure and in situ stress fields.

SITE GEOLOGY AND PHYSICAL PROPERTIES

Included in this investigation was a geological study of the four underground instrumentation sites (figs. 3-4), and the retrieval of core for physical properties testing (tables 1-2). The roof strata were sampled from 10 boreholes drilled during site instrumentation; stratigraphic columns for only the 2 headgate sites, middle entry roofs, are shown in figure 5. The immediate roof, a black silty shale varying in thickness from 1 to 3 ft, deteriorates with exposure to air, separates along thin bedding planes, and fractures into small blocks. Overlying the immediate roof are four sandstone beds, designated as "A" through "D" in ascending order. The A sandstone did not appear as a distinct unit in the panel 1 boreholes. The C sandstone, the thickest and most consistent unit, is present at the top of three of the boreholes. The upper sandstone unit, D, was not intersected in any of the boreholes.

Table 1.—Summary of physical properties tests

| Geological material and physical property | Minimum | Maximum | Mean | Number of samples |
|---|---------|---------|--------|-------------------|
| Black shale: | | | | |
| Compressive strength psi .. | 1,441 | ND | ND | 1 |
| Interbedded siltstone, black shale: | | | | |
| Compressive strength psi .. | 11,611 | 22,032 | 17,123 | 32 |
| Young's modulus (E) 10 ⁶ psi .. | 1.74 | 4.96 | 2.59 | |
| Poisson's ratio (μ) | 0.14 | 0.46 | 0.33 | |
| Interbedded sandstone, siltstone, black shale: | | | | |
| Compressive strength psi .. | 6,679 | 23,826 | 15,661 | 40 |
| Young's modulus (E) 10 ⁶ psi .. | 1.68 | 6.95 | 2.69 | |
| Poisson's ratio (μ) | 0.19 | 0.45 | 0.34 | |
| Sandstone: | | | | |
| Compressive strength psi .. | 7,933 | 30,819 | 14,939 | 26 |
| Young's modulus (E) 10 ⁶ psi .. | 1.93 | 6.89 | 3.21 | |
| Poisson's ratio | 0.12 | 0.48 | 0.31 | |
| Pyritic black shale: | | | | |
| Compressive strength psi .. | 13,704 | 17,762 | 15,717 | 12 |
| Young's modulus (E) 10 ⁶ psi .. | 2.42 | 3.08 | 2.75 | |
| Poisson's ratio (μ) | 0.30 | 0.47 | 0.36 | |

ND No data.

A northwest-trending normal fault intersected panel 1 between crosscuts 35 and 36 in the headgate and between

crosscuts 39 and 40 in the tailgate. In panel 1, the fault strikes at N. 26° W. and dips near vertical. The fault planes are less than 10 ft apart, and the coal seam is offset 6 ft. In addition to movement along fault planes, movement has occurred parallel to bedding planes in the roof, as evidenced by slickensides. The slickensides can be observed along a bedding plane, approximately 2 in above the coalbed, and indicate nonuniform direction of movement. Bedding plane movement is thought to have resulted from folding. Shear movement has created gouge zones and displacement within the Wadge coal seam; zone widths vary from less than 1 in to up to 10 ft, and the length varies from a few feet to 100 ft. Two shear zones intersect the headgate near sites H and B.

Table 2.—Summary of tensile strength tests

| Geologic material | Mean value, psi | Number of samples |
|---|-----------------|-------------------|
| Black shale | ND | ND |
| Interbedded siltstone, black shale | 765 | 11 |
| Interbedded siltstone, sandstone, black shale | 557 | 19 |
| Sandstone | 718 | 10 |
| Pyritic black shale | 579 | 6 |
| ND | No data. | |

The coalbed exhibits a prominent face cleat, striking northwest and dipping near vertical. The less well-defined butt cleat trends northeast, with a vertical dip varying 6°. Cleat spacing varied from 6 in to 2 ft, except in the shear zones where spacing decreased to less than 1 in. Cleat direction roughly parallels joint orientations and may indicate that local uniform stresses may have induced the formation of both the joints and cleats within the mine area. Rib behavior is apparently influenced by the cleat orientation. The north-south ribs, longwall face, and pillar crosscut ribs remained relatively intact and free standing, while the east-west ribs, those forming the panel ribs and pillar entry ribs, exhibited a greater degree of sloughage. While measurements of cleat shear strength were not made, directionally related yield zone development indicates that differences between the face and butt cleat strengths exist.

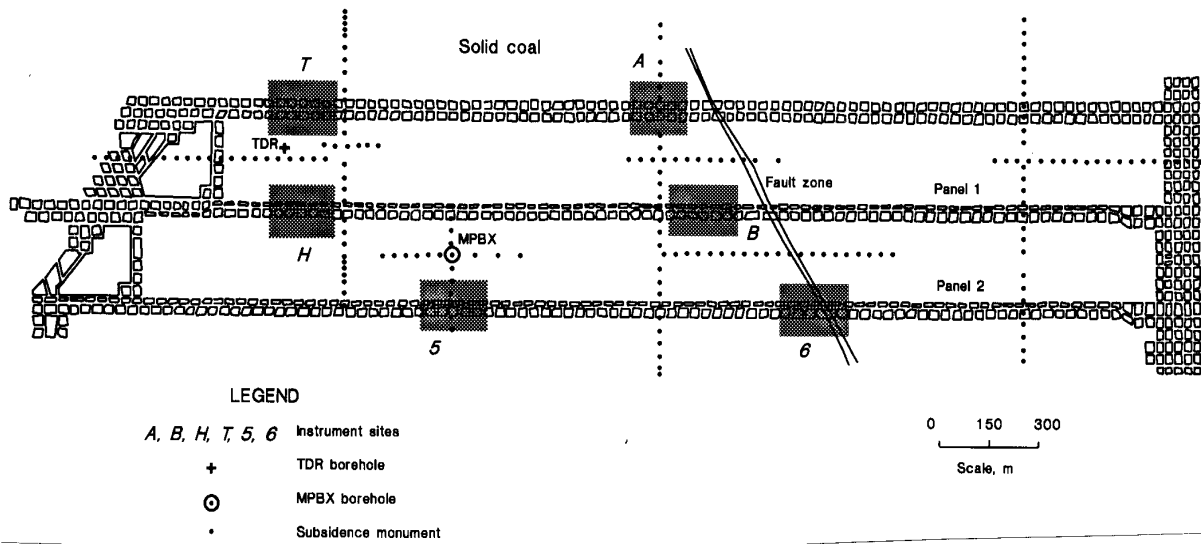


Figure 3.—Mine layout and study site locations, headgate sites *H* and *B* and tailgate sites *T* and *A*. (MPBX = multiple position borehole extensometer.)

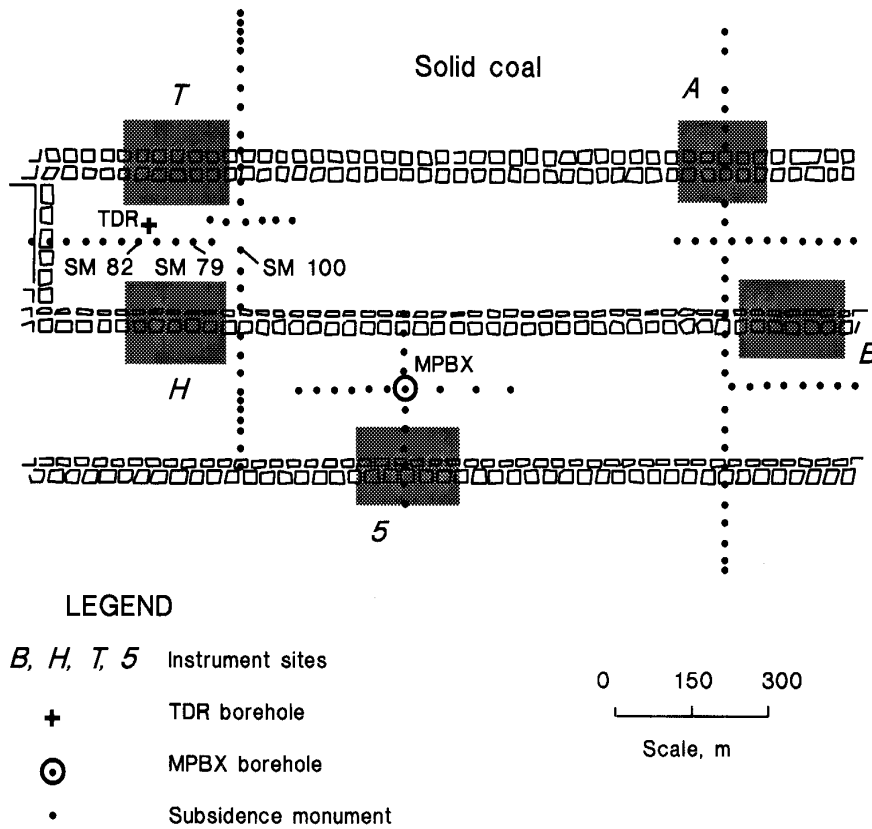


Figure 4.—Instrumentation location detail of panel 1, surface and subsurface. (MPBX = multiple position borehole extensometer.)

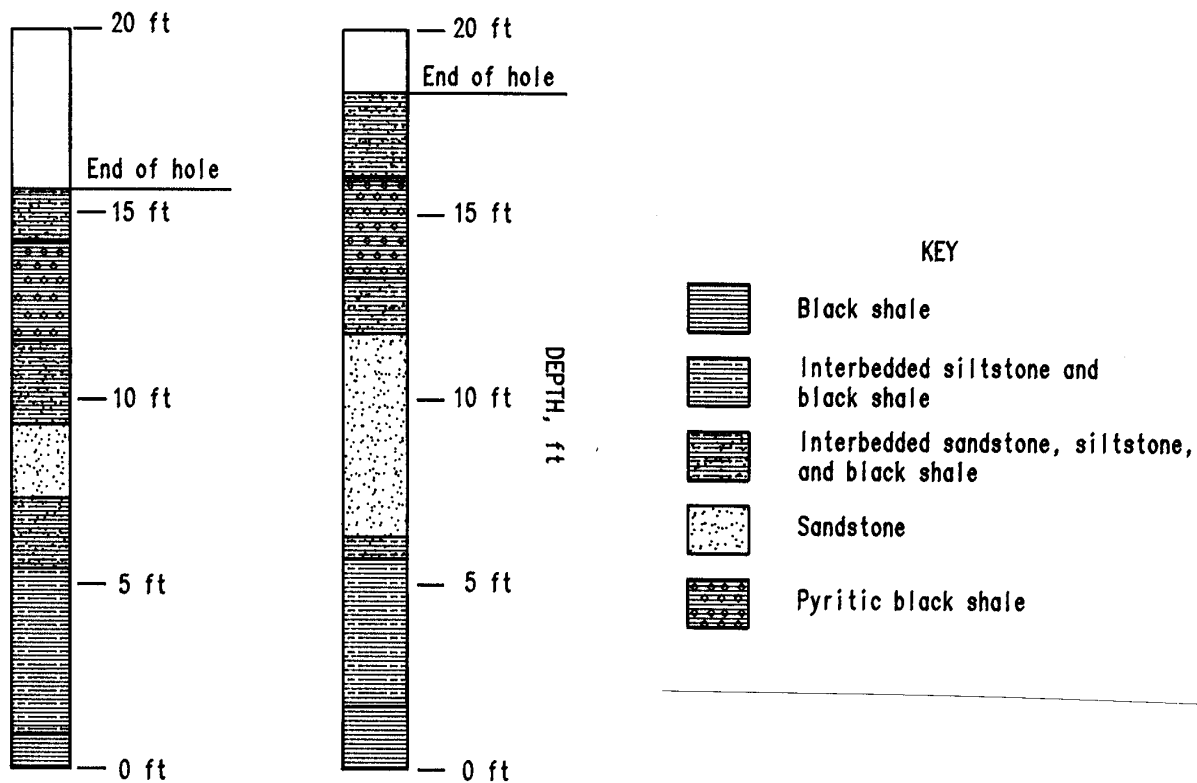


Figure 5.—Stratigraphic column of headgate sites of middle-entry roofs.

DATA ANALYSIS

The evaluation of strata response to panel 1 mining included characterization of main roof caving from TDR readings and surface subsidence measurements and mining-induced pressure changes from hydraulic pressure cells installed at the instrumentation sites shown in figures 3 and 4. Of particular interest were the behavior of the approximately 200-ft-thick Twentymile Sandstone, 700 to 750 ft above the coalbed, and the in-mine performance of the headgate chain pillars. Also included were analyses of mining-induced load transfers.

Underground instrumentation emphasized the use of encapsulated borehole pressure cells (BPC's) installed at four sites to monitor mining-induced pressures in the panel and adjacent chain pillars. Additional BPC's were installed in the adjacent panel and in the immediately north, solid coal to investigate load transfer; horizontal stresses were monitored from cells installed in the immediate roof. Figures 6 and 7 show detailed instrumentation layouts for headgate sites H and B, respectively, and figures 8 and 9 show the tailgate sites, T and A, respectively.

Roof caving was monitored via TDR surveys of a coaxial cable installed from the surface in a 1,050-ft-deep borehole located over the instrumented panel. Location of the TDR borehole and surface subsidence survey lines are shown in figure 4.

MAIN ROOF CAVING ACTION

Main roof caving was monitored from TDR surveys of a coaxial cable cemented into an approximately 1,050-ft-deep borehole over panel 1; figure 10 shows a typical TDR survey with a roof break. Recent developments in TDR signature interpretation include differentiation between tensile and shear failures (6). Tensile failure is indicated by a small but extended voltage reflection trough prior to the large, positive circuit reflection. Shearing, on the other hand, produces a distinctive negative voltage reflection spike prior to the large, positive open circuit reflection (7). A previous study over a partially pillared, room-and-pillar section at the mine determined that caving conditions were

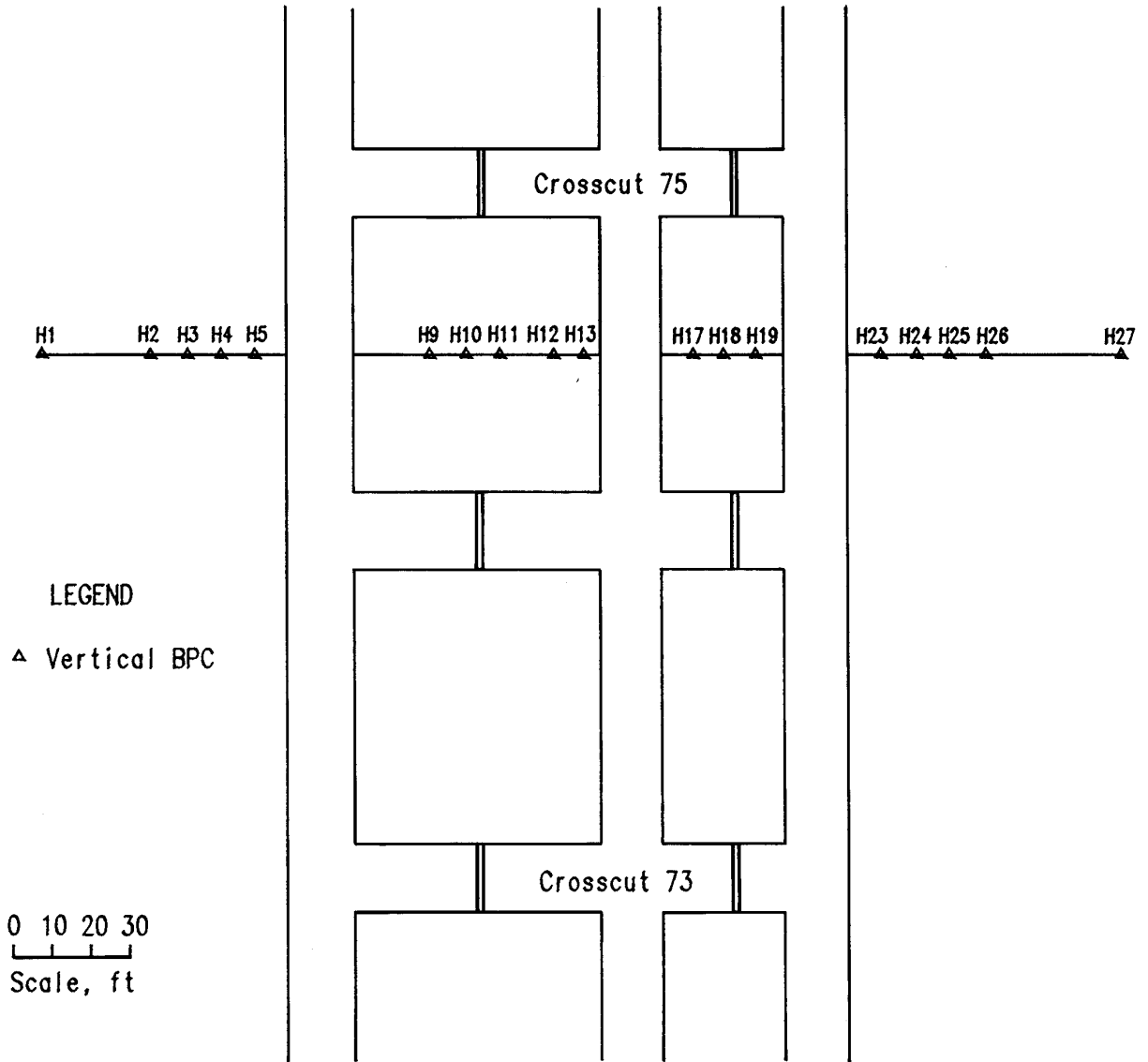


Figure 6.—Instrumentation detail of site H.

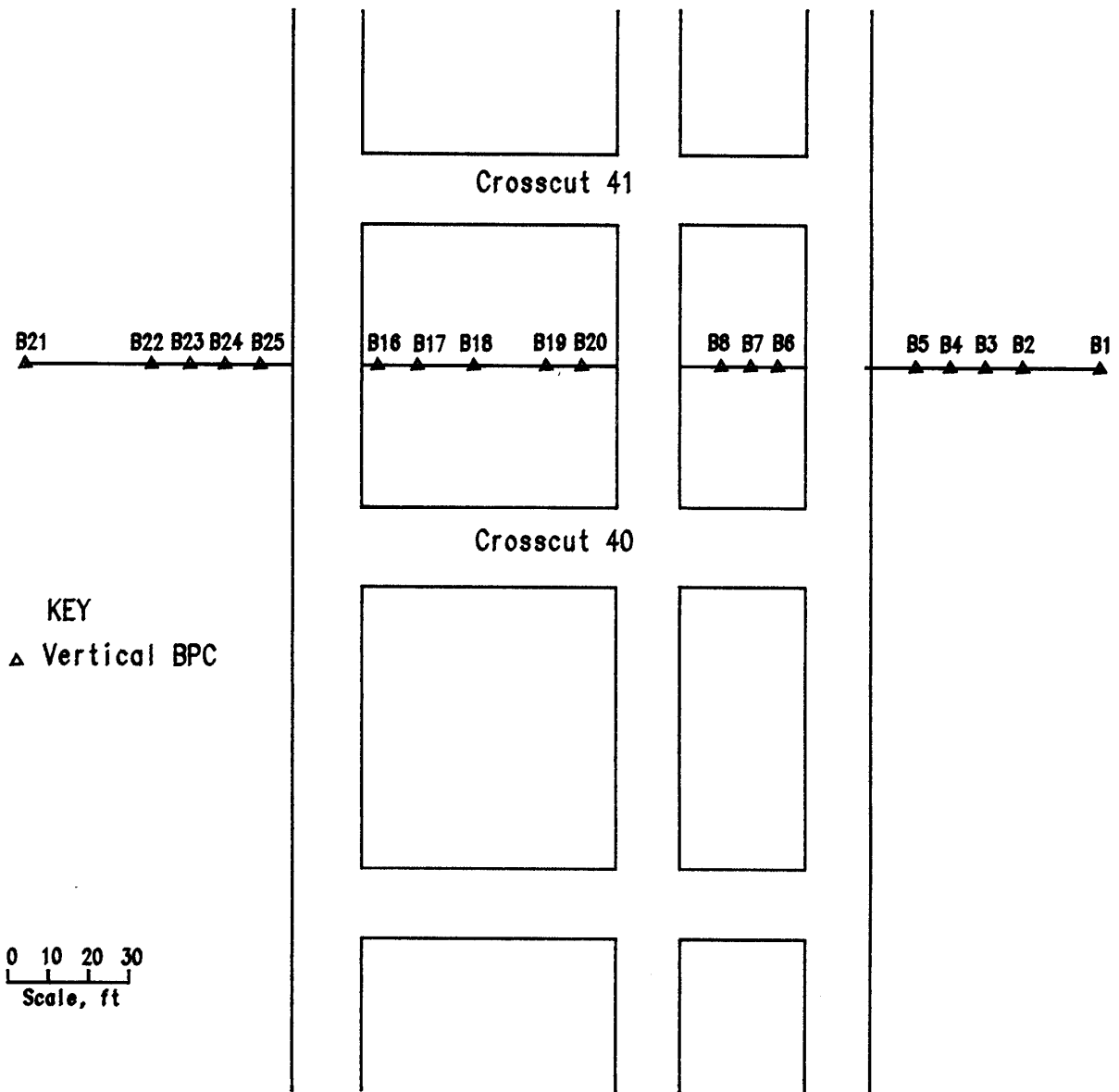


Figure 7.—Instrumentation detail of site B.

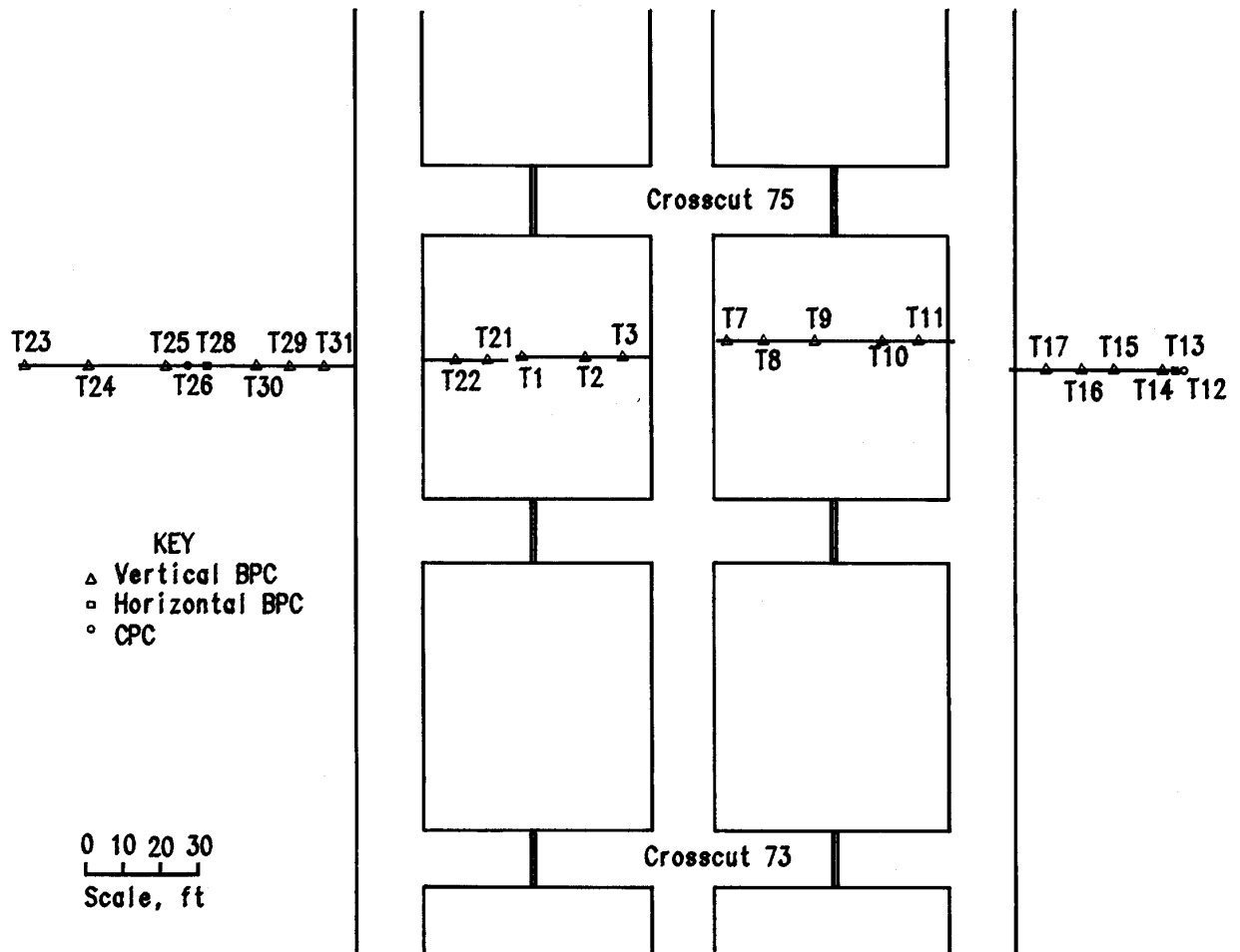


Figure 8.—Instrumentation detail of site T.

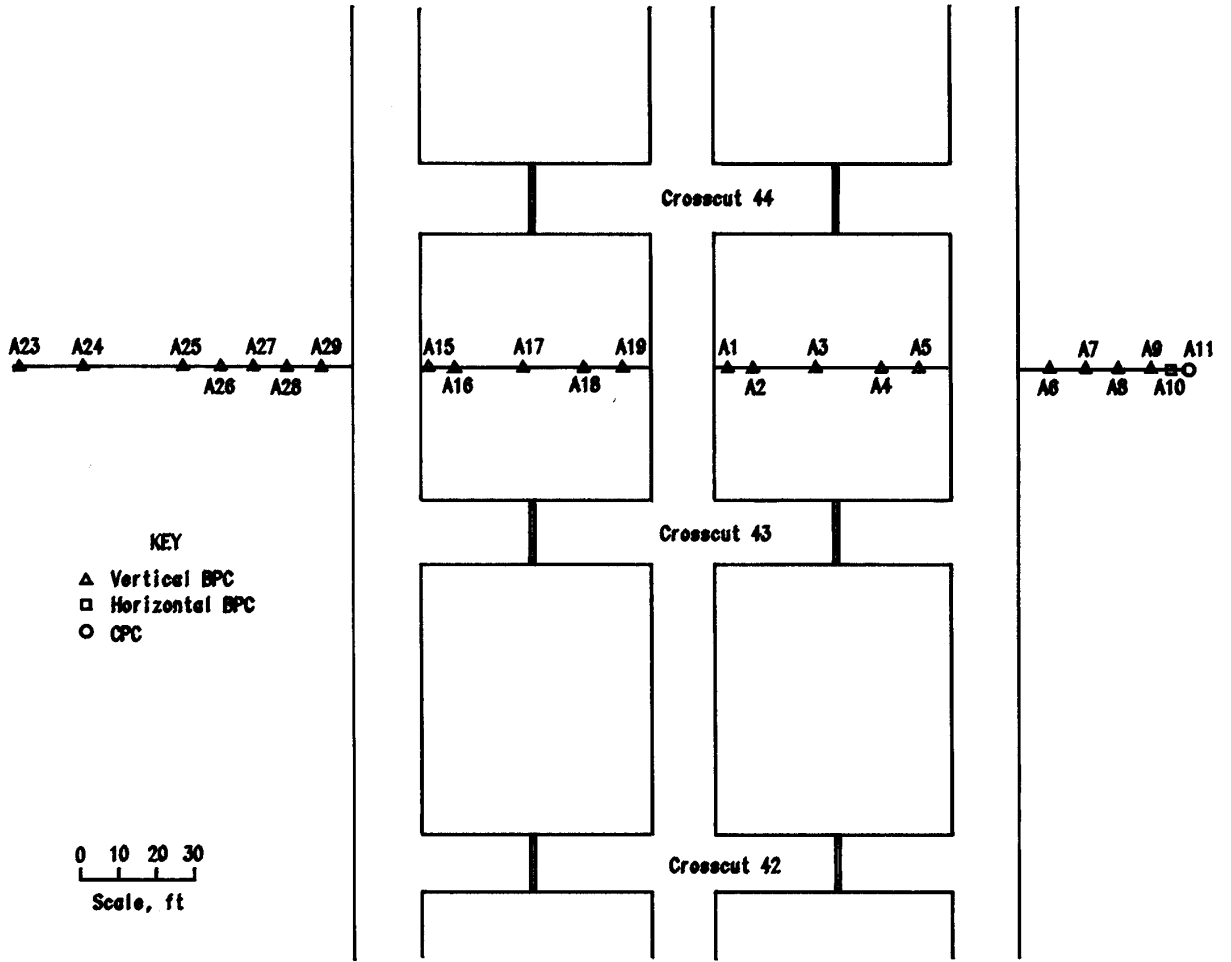


Figure 9.—Instrumentation detail of site A.

favorable. The approximately 10-ft-thick C sandstone unit, 10 to 15 ft above the coalbed, caved readily, and the main roof, with additional pillaring, collapsed. Based on these TDR surveys, this previous study indicated that early face support loads, corresponding to an 80-ft-thick roof, could be expected (4).

Data from the TDR surveys over panel 1 indicated that roof movement began almost immediately after passage of the face and was essentially completed within 2 weeks after mining (fig. 11). Six distinct caving events were observed. Events 1 through 3, at depths of 720, 640, and 540 ft, within the Lewis Shale began caving soon after face passage. This lower roof caving phase was completed within 6 days after face passage, a face distance of about 130 ft. The fourth distinct cave, 240 ft deep, on day 7 marked the failure of the 150- to 200-ft-thick Twentymile Sandstone. This failure occurred when the face had retreated approximately 150 ft outby. Total retreat at this point was about 600 ft. Subsequent failures in the overlying shale members occurred until the face retreated approximately 350 ft outby the TDR borehole; readings were terminated at this time. Included with figure 12 are subsidence data from surface monument SM 82, closest to the TDR borehole. With retreat of the face, subsidence accelerated as the cave zone ascended, especially after the failure of the Twentymile Sandstone and the overlying strata. During the surface subsidence monitoring period shown in figure 12, a maximum subsidence of 2.98 ft was measured; during panel 1 mining, SM 82 subsided over 4 ft.

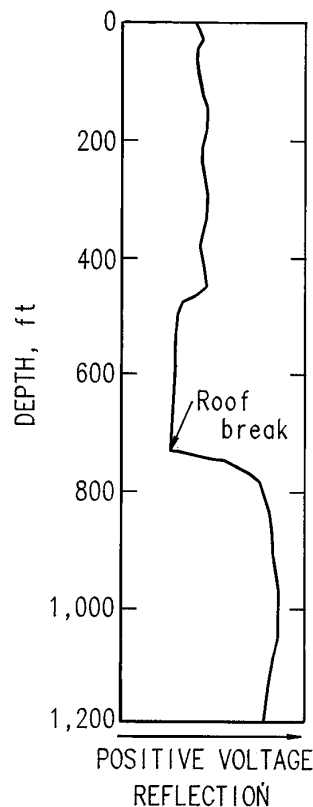


Figure 10.—Typical TDR survey with tensile roof break.

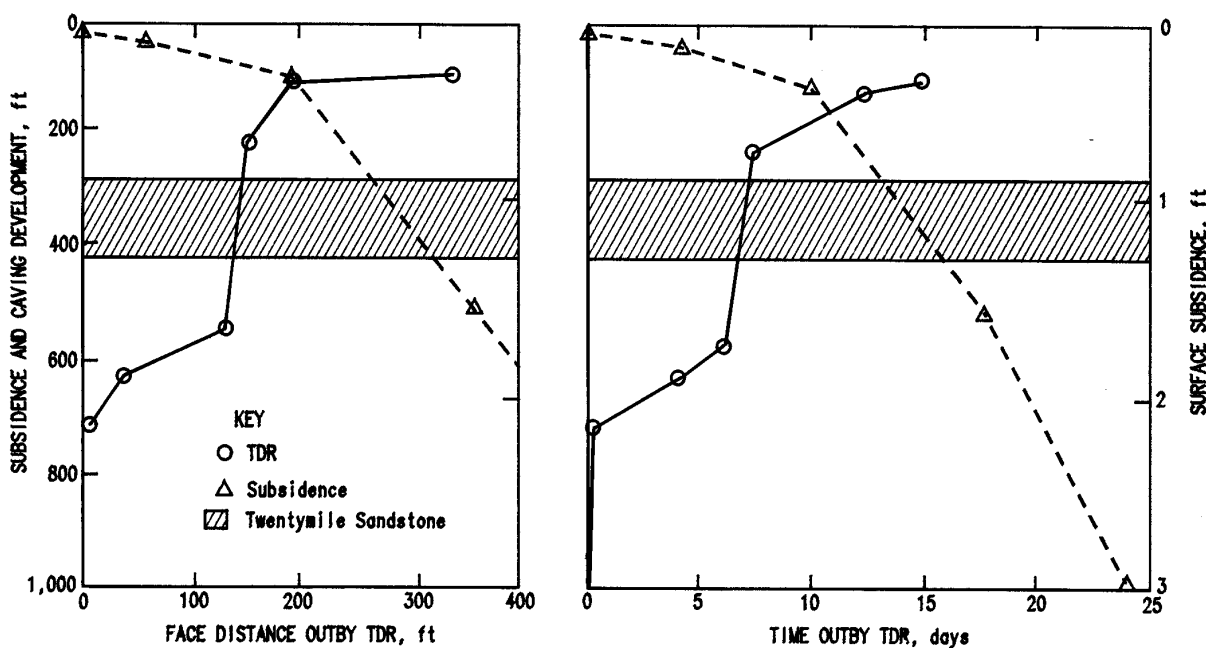


Figure 11.—Main roof caving of panel 1 versus face distance and time.

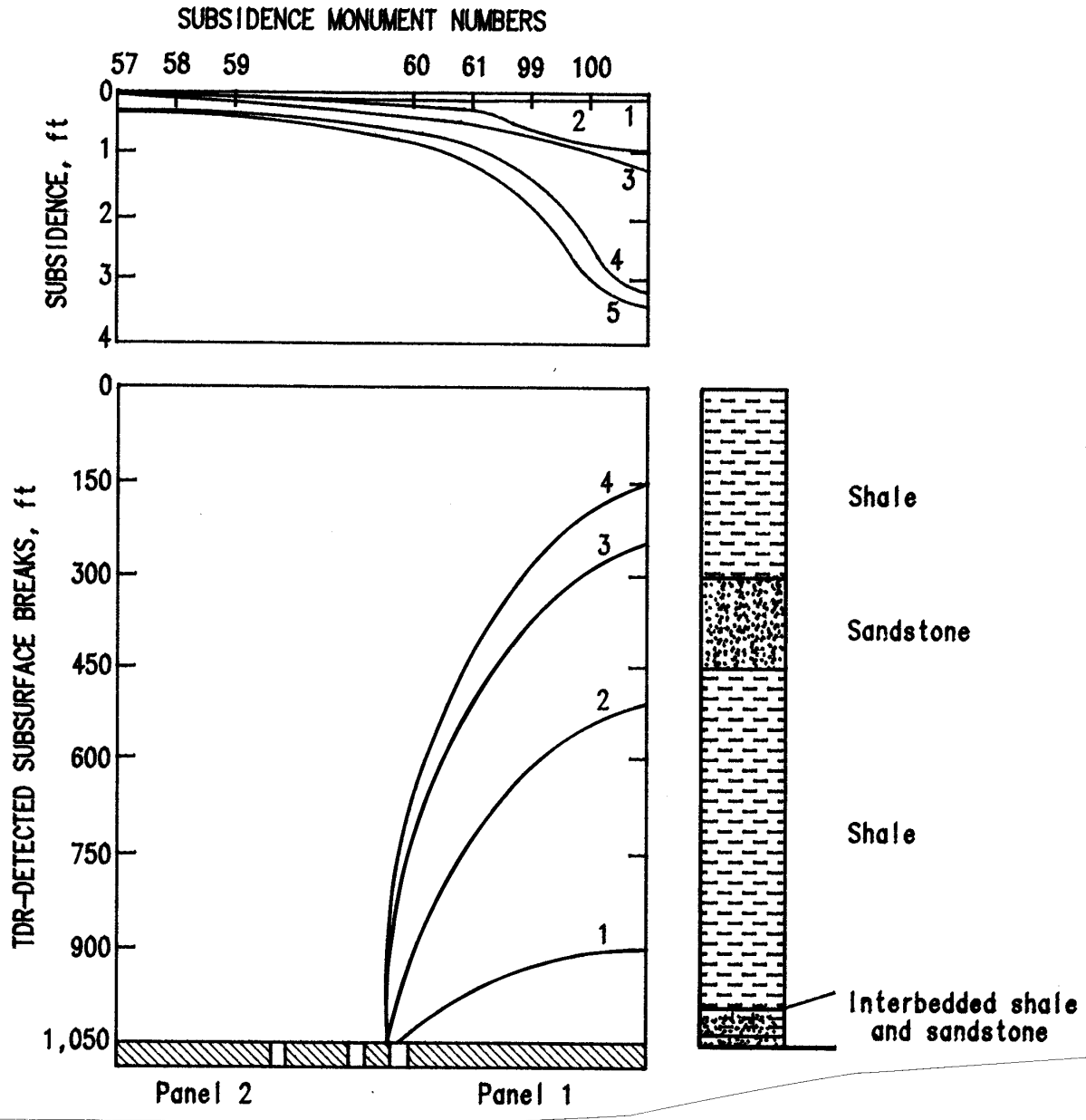


Figure 12.—Suggested sequence of main roof caving. Curves 1 and 2 represent roof movement due to initial caving as the face passed; curve 3 results from failure of the main roof sandstone unit; curves 4 and 5 occur as the upper roof units subside onto the consolidating gob.

Main roof caving was investigated not only to characterize subsurface failures but also to correlate, if possible, roof action with observed pillar behavior, especially load transfers between the headgate chain pillars and between the pillars and the adjacent panel 2. Since the TDR borehole, surface subsidence line B, and the underground instrumentation sites H and T (fig. 4), were not superimposed, the following assumption was made. Since surface subsidence results from subsurface caving, similar surface subsidence development curves should reflect similar subsurface caving. To test this assumption, subsidence development curves were plotted for three stations located over the panel 1 axis: SM 82, closest to the TDR borehole; SM 79, in line with the subsurface instrumentation sites; and SM 100, part of survey line B (fig. 4). Subsidence development curves versus outby face distance and elapsed time are shown in figure 13. Included with this figure is the subsidence development curve for SM 106, part of the survey line closest to the outby sites A and B. Figure 13 indicates a very close agreement between the three inby monuments—SM 79, SM 82, and SM 100—and with SM 106 above the outby instrument stations. Since the subsidence development curves agreed so closely, it was concluded that the following roof action occurred (fig. 12). With retreat of panel 1 (curves 1 and 2), arching over the cavity and surface subsidence occur. With failure of the Twentymile Sandstone (curve 3) and the overlying strata (curve 4), the arch fails and surface subsidence accelerates. Continued subsidence occurred as the gob consolidated (curve 5).

PRESSURE MEASUREMENTS

Mining-induced pressures were measured using encapsulated BPC's installed in panel 1, the headgate and tailgate chain pillars, the adjacent panel, and in the solid instrumentation sites immediately north of the tailgate (fig. 3).

Pressure cell data analysis included (1) characterization of the forward abutment, (2) in situ yield pillar behavior and comparison to design techniques, and (3) yield pillar-abutment pillar load transfer.

Forward Abutment Studies

The vertical component of the forward abutment was measured using BPC's installed in the panel 1 headgate and tailgate ribs. Figures 14 through 16 show the measured pressures versus face distance. The tailgate rib also included a stress site consisting of two BPC's, one to measure vertical pressure and the other to measure horizontal pressure, and one cylindrical pressure cell (CPC) to measure radial pressures.

Figures 14 through 16 include inserts of pressure profiles into the panel 1 rib at a 0-ft face distance. For comparison, these profiles are combined in figure 17. Measurements generally agree with previous western U.S. coal mine studies in that forward abutment pressures begin when the face approaches to within 1/4 to 1/3 ft of the depth, and at approximately 0.1 ft of the depth, there are accelerated pressure increases (8-11). However, unlike

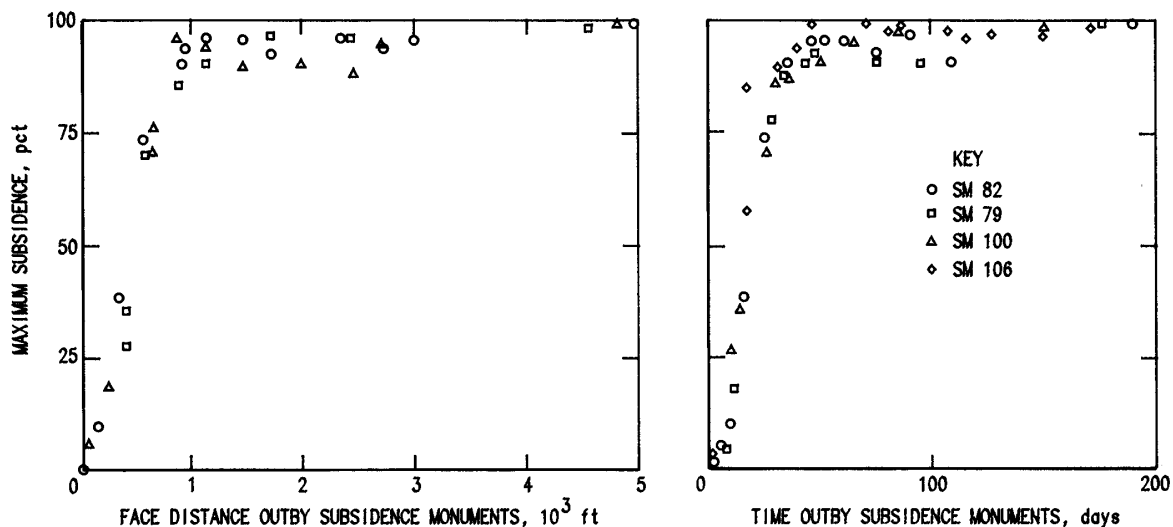


Figure 13.—Subsidence development versus face distance and time.

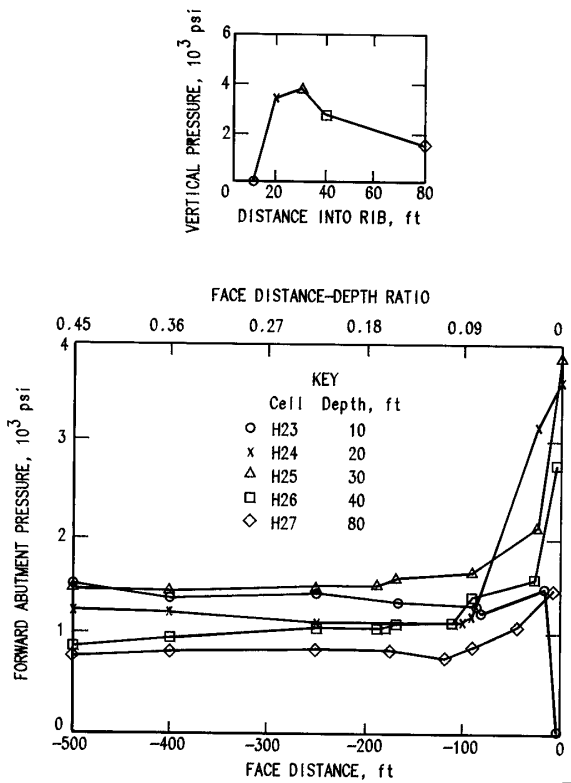


Figure 14.—Forward abutment pressure at headgate site H.

previous studies that indicate, through rapid vertical pressure losses, yielding at about 0.01 ft depth into the face, no evidence for development of a significant yield zone at this mine exists. For sites H and T, only the cells at the panel edges (those installed at 10 ft inside the rib) indicate yielding at the 0-ft face distance. The other site H and T cells continued to increase and, as shown in figures 14 through 16 inserts, the panels depict an essentially elastic stress distribution. The outby sites A and B indicated continued pressure increases and did not show yielding, even for the 10-ft-depth cells (fig. 17).

Figure 17 summarizes the "final" pressure readings versus cell depth into the panel 1 rib. While differences exist between these final pressure profiles, they agree that the longwall panel, to a depth of 100 ft within the ribs, retained vertical pressure and did not yield as the face approached. Yielding, where observed, was limited to approximately 10 ft inside the panel rib. The data indicate some differences between the inby sites H and T and the outby sites A and B. The peak pressures at sites H and T

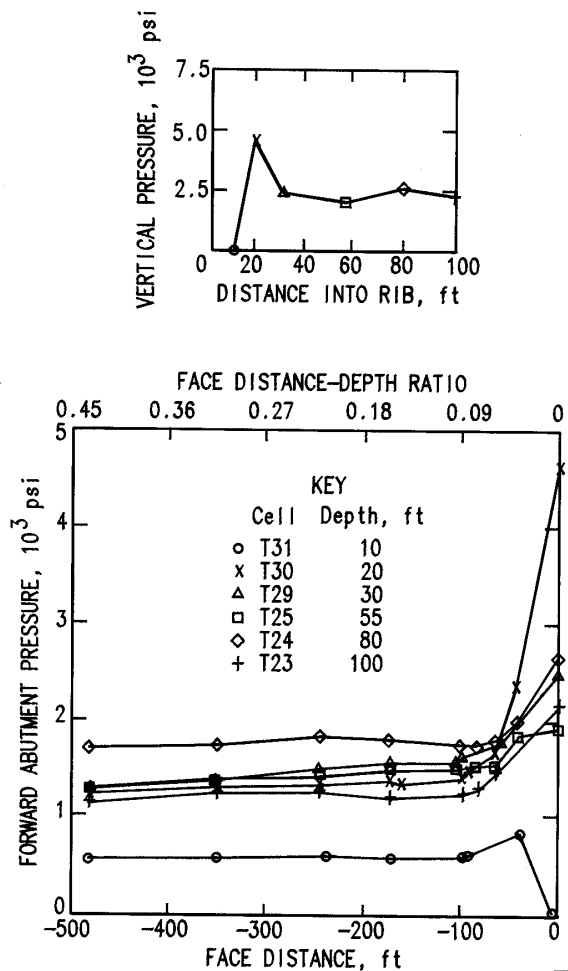


Figure 15.—Forward abutment pressure at tailgate site T.

exceeded those at sites A and B; however, these higher pressures probably result from the fact that the 10-ft-depth cells yielded and pressure redistribution within the face occurred.

Forward abutment effects were also monitored from a three-cell stress site installed in the panel 1 tailgate rib. Measurements from the stress site, consisting of one CPC and two BPC's, are shown in figure 18. The stress site data also indicate the absence of a significant yield zone within the face; while the horizontal cell (T28) shows a pressure drop just prior to cutting by the shearer, the vertical cell (T25) continued to increase until the BPC was cut.

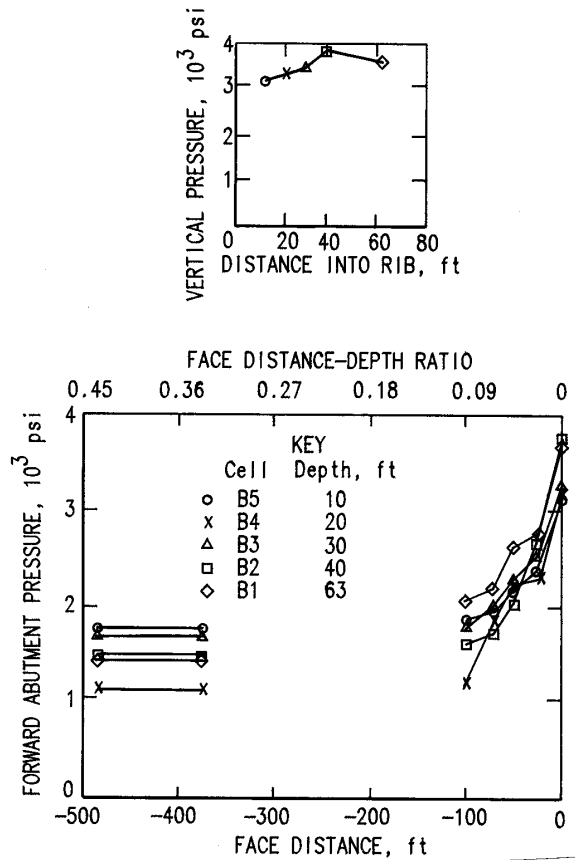


Figure 16.—Forward abutment pressure at headgate site B. Gap in pressure data occurred during relocation of instrument monitoring station.

During panel 1 mining, coal ejected from the face necessitated the wearing of protective clothing. Using the stress site data and a method proposed by Lu (12-13) to convert cell pressures to absolute ground stresses, it appears that the mining-induced stresses are insufficient to induce significant fracturing of the face. Figure 19 shows a Mohr's circle generated from conversion of cell pressures to ground stresses versus failure envelopes developed from testing of the Wadge coal seam. While the cell T25 vertical pressure reading is low compared with that of the adjacent cells (figs. 15, 18) and could modify the ground stress calculations, the calculation of nonfailure agrees with other measurements that indicate that a significant yield zone did not occur.

Horizontally oriented BPC's were not installed with the other cells at this site. Since Lu's technique requires

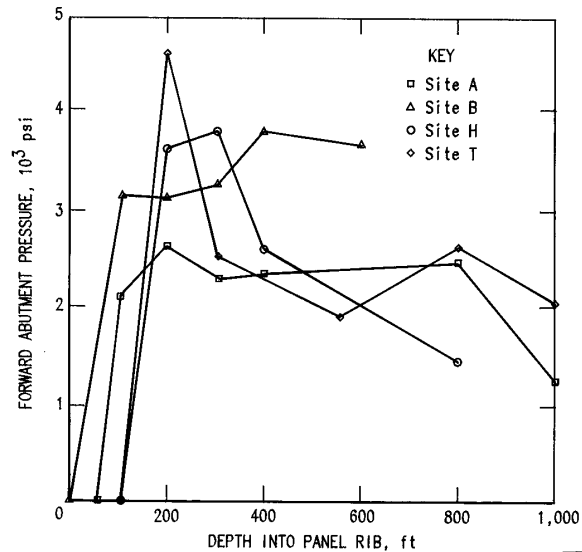


Figure 17.—Stress profiles of panel rib at 0-ft face distance.

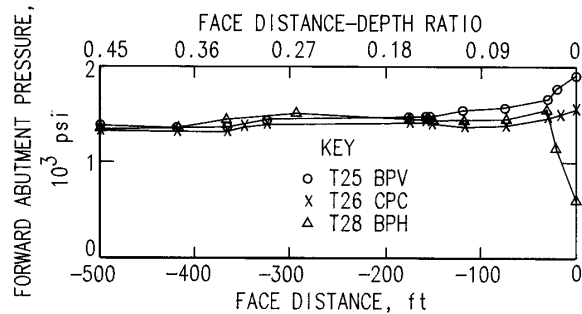


Figure 18.—Forward abutment pressure of stress site at site T. (BPV and BPH designate borehole pressure cells oriented to measure vertical and horizontal pressures, respectively.)

horizontal pressure cell readings for each vertical cell, calculation of ground stress for the other tailgate rib cells was not made.

Yield Pillar Behavior

The panel 1 three-entry headgate included a 35-ft-wide yield pillar adjacent to the panel and an 80-ft-wide abutment pillar. The yield pillar was sized to yield with panel 1 mining. The abutment pillar was sized to withstand first panel mining-induced loading yet yield with panel 2 mining. Yield pillar studies included evaluation of pressure

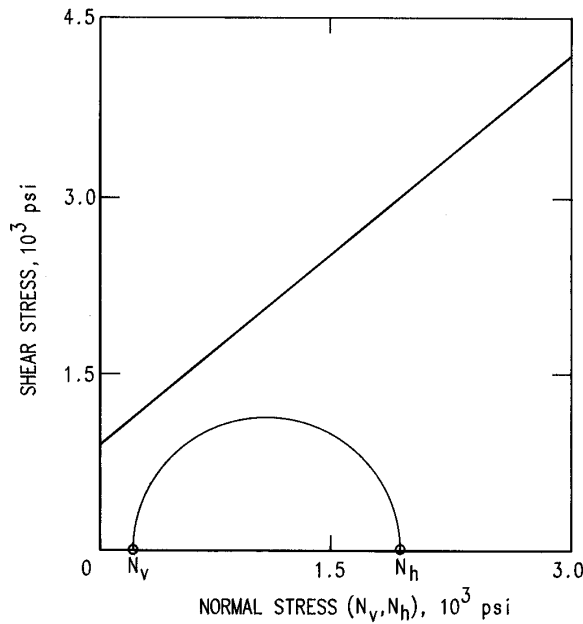


Figure 19.—Stress state from cell readings at 0-ft face distance. Slope of failure envelope corresponds to a friction angle of 36°.

cell data and a comparison between in-mine and predicted behavior.

Two yield pillars, sites H and B at crosscuts 75 and 40, respectively, were monitored to compare design versus in-mine behavior. Pillar pressures versus face distances are shown in figure 20. Despite poor cell response from one BPC installed in each pillar, the observed loading histories suggest similar pillar responses.

The site H pillar indicated increased loading with approach of the face and reached maximum pressure when the face was 300 ft outby. Maximum vertical pressure (5,200 psi) was reached on the rib nearest panel 1 and decreased with distance into the pillar. Between 300 and 500 ft, both ribs crushed out and the pillar retained a stressed core. Cell H17 responded poorly, despite repairs and repressurization. However, based on H18 and H19 data, the pillar appeared to respond elastically until yielding and a central, stressed core remained.

Pillar B (fig. 20), also indicated an elastic response to mining, prior to crushing out. Poor cell response (B7), prevented determination of whether the pillar also contains a stressed core. Although two BPC's responded poorly, the pillars generally indicate similar behavior. Cells H19 and B8, nearest panel 1, show their highest stresses at face

distances of 250 to 300 ft, and both pillars yielded by a distance of 500 ft.

A previous study at another western U.S. coal mine observed that very local conditions, e.g., variations in roof, floor, and coal properties, influenced pillar yielding. Two design approaches were compared to the in-mine design, sized to yield with panel 1 mining. Results using Wilson's (14-15) expressions for both rigid roof and floor and for yielding roof and floor conditions (equations 1 and 2, respectively) were calculated as follows and are shown in figure 21A:

$$W = 2 \frac{m}{F} \ln \left(\frac{q}{p + \hat{p}} \right), \quad (1)$$

and

$$W = m \left[\left(\frac{q}{p + \hat{p}} \right)^{\frac{1}{k-1}} - 1 \right], \quad (2)$$

where W = yield pillar width, ft,

m = pillar height, ft,

q = overburden pressure, ft,

$$F = \left(\frac{k-1}{\sqrt{k}} \right) + \frac{(k-1)^2}{k} \tan^{-1} \sqrt{k},$$

p = artificial edge constraint,

\hat{p} = failed coal uniaxial strength, 1 ton/ft²,

$$k = \frac{1 + \sin \phi}{1 - \sin \phi},$$

and ϕ = friction angle, deg.

Figure 21 indicates the required yield pillar widths for both the rigid and the yielding roof and floor conditions. Since the roof consisted primarily of a black silty shale that deteriorated with exposure to air and required mesh for supplemental support and since the immediate floor did not contain massive, stiff strata, the yielding roof-floor condition most accurately simulates in-mine conditions. The yielding condition curve indicates that the 35-ft-wide yield pillar nearly matches the size required from the Wilson (14-15) method. Pillar pressure data suggest the existence

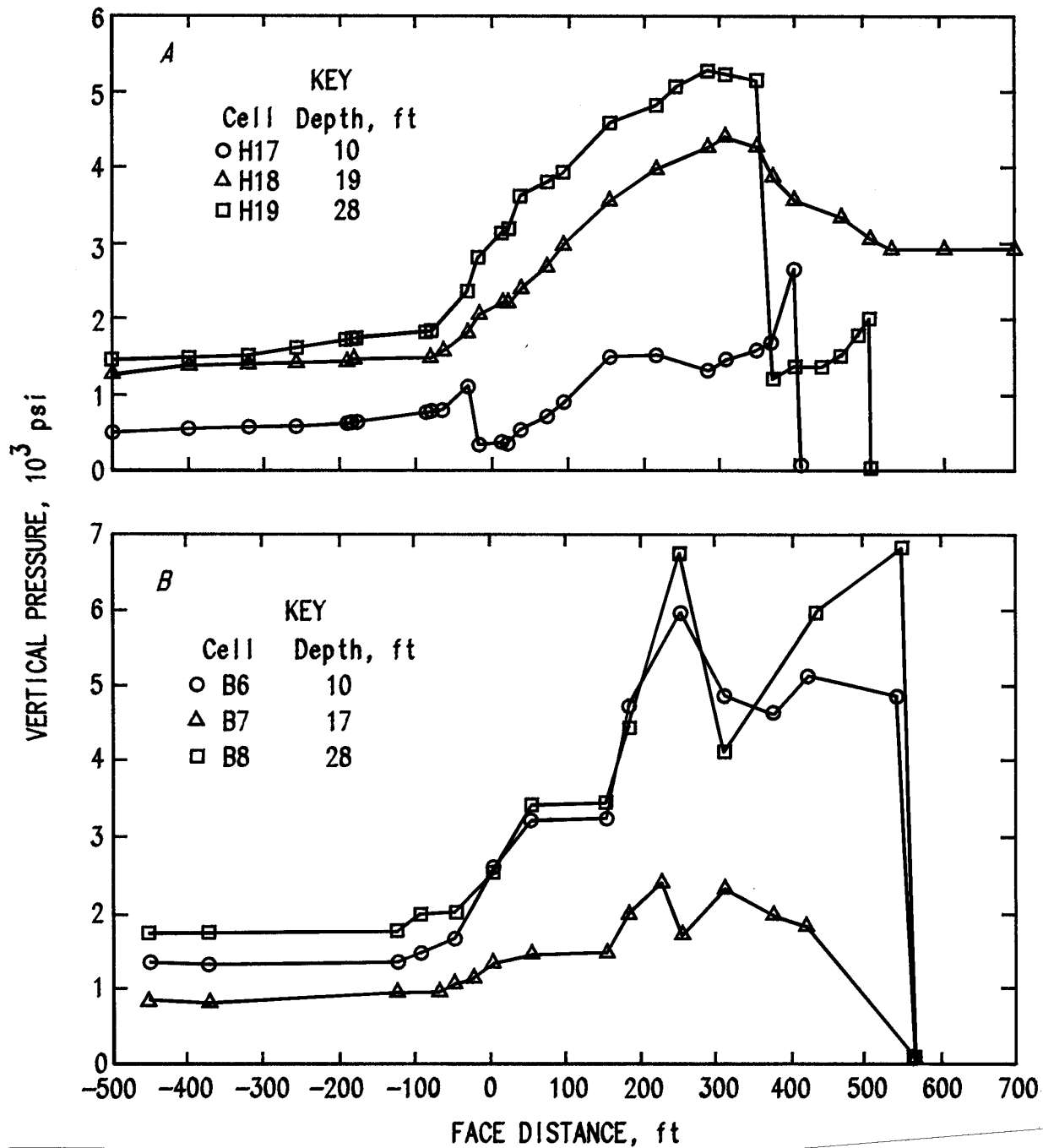


Figure 20.—Vertical pressure readings in yield pillars. A, Site H (crosscut 75); B, site B (crosscut 40).

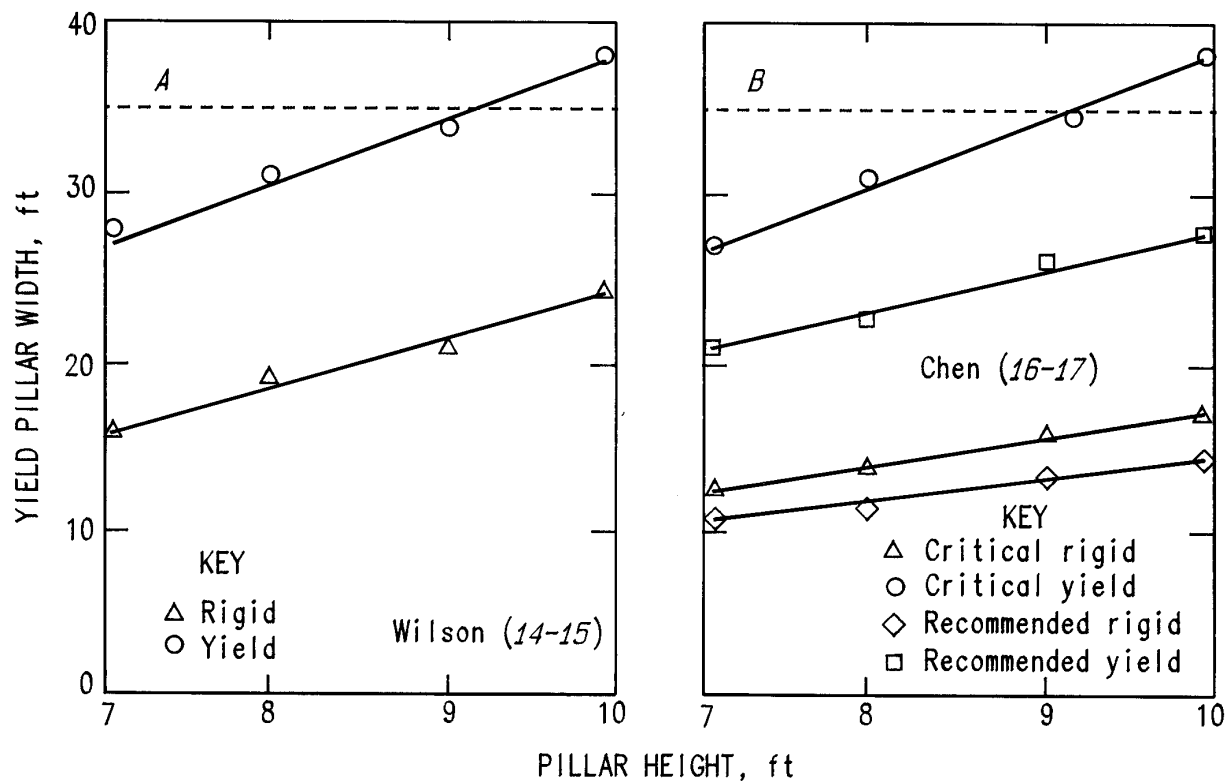


Figure 21.—Comparison of estimated yield pillar width, Wilson (A) versus Karmis-Chen (16-17) (B) approach.

of a stressed pillar core. Since the actual and required pillar widths are so close, it appears that the 35-ft-wide pillar may represent a critical or maximum yield pillar width.

Since one pillar indicated a stressed central core, a yield pillar design method proposed by Karmis (16) and Chen (17) was investigated to determine critical width. This technique includes friction angle, Poisson's ratio, and pillar geometry functions to size both a critical yield pillar width (one containing a central stressed core), and a "recommended" width (one having a peak stress equal to the tributary pressure).

Using the following expressions, the same friction angle (35.6), and a Poisson's ratio range of 0.30 to 0.40, maximum or critical yield pillar and recommended widths were determined (fig. 21):

$$W = 2m \left\{ 9.61 \cdot \cos \left[\frac{1}{3} \cos^{-1} \left(\frac{\gamma h \cdot 10^{-5}}{f(k)f(\mu)} - 1 \right) \right] - 4.8 \right\}, \quad (3)$$

where W = yield pillar width, in,

m = pillar height, in,

γ = overburden density, pci,

h = depth, in,

$f(k) = k^{1.7}$,

and $f(\mu) = -0.028 + 0.057 \mu + 0.17 \mu^2$, where μ = Poisson's ratio.

Figure 21 indicates that at the lower Poisson's value (0.30) and corresponding to Wilson's (14-15) yielding roof and floor conditions, yielding should occur. The 0.40 ratio case, corresponding to the rigid condition, indicates that smaller pillars would be required, and as seen using the previous approach, property variations can significantly

affect yield pillar sizing. This approach was also used to determine a recommended pillar size, a pillar where maximum core pressure equals tributary pressure, by solving iteratively

$$\sigma_t = k \cdot f(k) \cdot f(\mu) \cdot f\left(\frac{W}{2m}\right),$$

$$\text{and } f\left(\frac{W}{2m}\right) = 6545 \left(\frac{W}{2m}\right)^2 + 454 \left(\frac{W}{2m}\right)^3, \quad (4)$$

where σ_t = tributary pressure.

Figure 21 shows the recommended yield pillar widths for the rigid and yielding end conditions. At the in-mine 9-ft pillar height and 0.30 Poisson's ratio, the recommended pillar width is about 26 ft. Figure 21 illustrates a comparison between the methods. Under yielding roof and floor conditions, the methods calculated from the properties used nearly identical maximum yield pillar widths. Both indicate that not only should the 35-ft-wide pillars yield, but that they are near critical width. The rigid condition pillar widths should be less than 20 ft; however, the

assumption of rigid roof and floor does not represent in-mine conditions.

Summarizing yield pillar behavior with the proviso that poor response by two BPC's makes firm conclusions more difficult, it appears that (1) the 35-ft-wide pillars yielded following face passage; (2) the pillars are probably near critical width and could possibly be reduced in width to induce, if wanted, earlier yielding; and (3) the presented design techniques accurately estimate required pillar widths. However, they are sensitive to coal properties and may require site-specific testing to "fine tune" the design.

Load Transfer Mechanisms

Load transfer between chain pillars and from the chain pillars onto panel 2 were investigated to determine panel 1 effects on the future panel 2 tailgate, to determine abutment pillar loading resulting from yielding of the smaller chain pillar, to assess roof behavior, and to correlate, if possible, observed pillar loading to the suggested main roof action.

Site H readings during panel 1 mining are summarized in figure 22. The profiles were generated to show mining-induced pressures during distinct phases: the forward

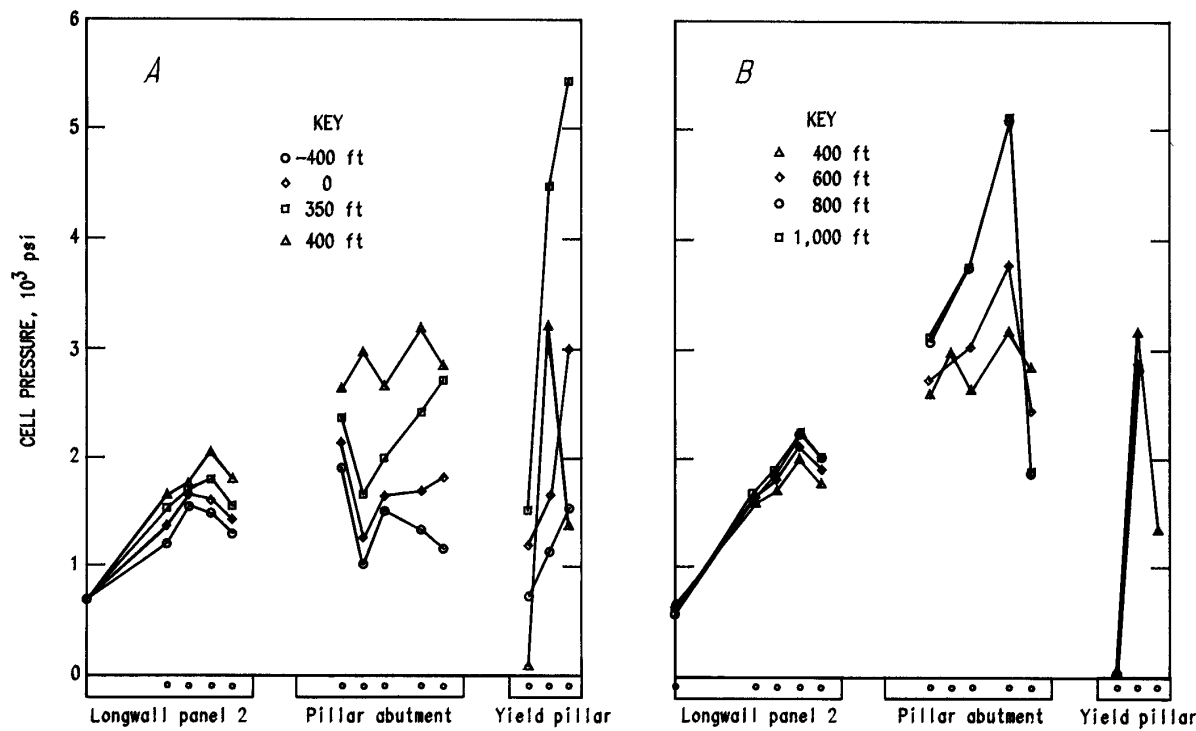


Figure 22.—Stress profiles at headgate site H.

abutment phase, -400 to 0 ft; side-abutment phase, to approximately +400 ft; and a postmining phase, to 1,000 ft. The side-abutment phase was divided to investigate any abutment pillar loading resulting from yielding of the smaller, adjacent chain pillar.

Forward abutment effects were mainly confined to the yield pillar and to the panel-side half of the larger chain pillar. Smaller (up to 100 psi) increases were measured on the panel 2 tailgate rib; these occurred on the outer 40 ft of the panel. Forward abutment extent decreased with distance from panel, and the panel entry system responded elastically to panel 1 mining. Average yield pillar pressure (mean of the BPC readings) increased from about 1,100 to 1,900 psi, a 73-pct increase in mean pressure. Abutment pillar pressure increased from 1,375 to 1,700 psi, a 23-pct rise over premining average BPC pressure. Panel 2 increases were on the order of 6 pct.

The side-abutment phase encompasses pressure changes measured between the 0-ft and +400-ft face distances. During this period, maximum yield pillar pressures occurred prior to failure. Abutment pillar pressure increases, due to main roof loading and load transfer from the yield pillar, and the panel 2 tailgate rib-pressure increases continued. Figure 22 includes two pressure profile lines, the maximum yield pillar pressure at about 350 ft and a postyield pressure profile at 400 ft. The preyield profile (350 ft) continued to show an elastic response to panel 1 mining. Maximum pressure occurred on the small pillar and decreased toward panel 2. Average small pillar BPC pressure increased to about 3,875 psi, an approximate 2,700-psi mean pressure increase (250 pct) over premining pressure. The abutment pillar continued to respond elastically, showing a mean BPC pressure of 2,200 psi, an 825-psi average cell pressure increase, or 100 pct over premining levels. The panel 2 tailgate showed minimal loading, an approximate 200-psi, 18 pct-increase over premining levels.

From 350 to 400 ft, the small yield pillar failed and apparently transferred load onto the adjacent abutment pillar and the panel 2 tailgate rib. During this period, yield pillar cell readings decreased drastically; pressures decreased about 4,000 psi on the rib nearest panel 1 and to 0 psi on the farthest rib. Core pressure dropped to 3,200 psi, but eventually stabilized. Average yield pillar cell readings dropped from a maximum 3,875 to 1,650 psi, but were still higher than the premining level (1,100 psi). Mean abutment pillar stresses increased to 2,830 psi, a 600-psi increase, and show loading of the pillar core. Small increases (less than 200 psi) continued to accumulate on the panel 2 rib.

With retreat of the face (fig. 22), yield pillar core pressure stabilized at about 2,900 psi. Between 400 and 600 ft, the abutment pillar began to show evidence of rib yielding. Readings inside the rib closest to the yield pillar

indicate a 900-psi drop that was accompanied by pressure increases in the abutment pillar core. Except for minor stress changes between the 800- and 1,000-ft distance readings, abutment pillar stresses evidently stabilized at 800 ft. The panel 2 rib continued to experience pressure increases; a maximum pressure of 2,300 psi was measured at 20 ft inside the rib.

The headgate site B data are summarized in figure 23. As seen at site H, the forward abutment induced an elastic response to panel 1 mining. Pressure increases were greatest on the small pillar and decreased with distance from panel 1. Small chain pillar average cell pressure increased to 2,540 psi, a 95-pct increase over the premining average (1,300 psi). Abutment pillar pressure increased to 1,830 from 1,630 psi, a pressure change increase of 12 pct. Panel 2 tailgate rib loading was minimal, a pressure change increase of 5 pct. The site B small chain pillar yielded with face passage; however, unlike the site H pillar, the postpeak stress phase lasted from about 250 to 550 ft. During this maximum pressure phase, yield pillar cell pressures approached 7,000 psi just before failing. With small pillar yielding, significant pressure increases occurred on the abutment pillar; the average cell pressure increased by approximately 800 psi, to 3,100 psi. Average pillar cell pressure change at this time was about 1,500 psi, a 90-pct increase over premining average cell pressure. With face passage to about 900 ft outby site B, pillar loading stabilized. From 560 to 900 ft, pressure changes were generally less than 100 psi. The abutment pillar still exhibited very high rib stress (approximately 8,000 psi) and remained elastic. Panel 2 continued to indicate high rib stress at 20 ft (2,800 psi). Figure 24 summarizes the pressure change percentages resulting from the four phases: forward abutment, peak small pillar pressure, postyielding, and postmining.

Figure 24 indicates good agreement for average cell pressure changes between sites H and B, especially prior to small chain pillar yielding. Previously discussed poor cell response from two BPC's may account for the larger decrease in the site B yield pillar. Prior to yielding, the sites exhibit very close agreement between average cell pressure increases and the distinct mining phases: the panel tailgate increases were 16 and 18 pct, abutment pillar increases were 60 and 42 pct, and yield pillar increases were 252 and 270 pct.

The previously presented analysis of main roof caving action determined that several distinct caving phases occurred (figs. 11-13). When the face was approximately 150 ft outby, the TDR data indicated that failure of the Twentymile Sandstone had occurred and that complete collapse of the cavity occurred when the face was about 350 ft outby. Additional retreat of the face resulted in continued subsidence, probably due to compaction of the gob.

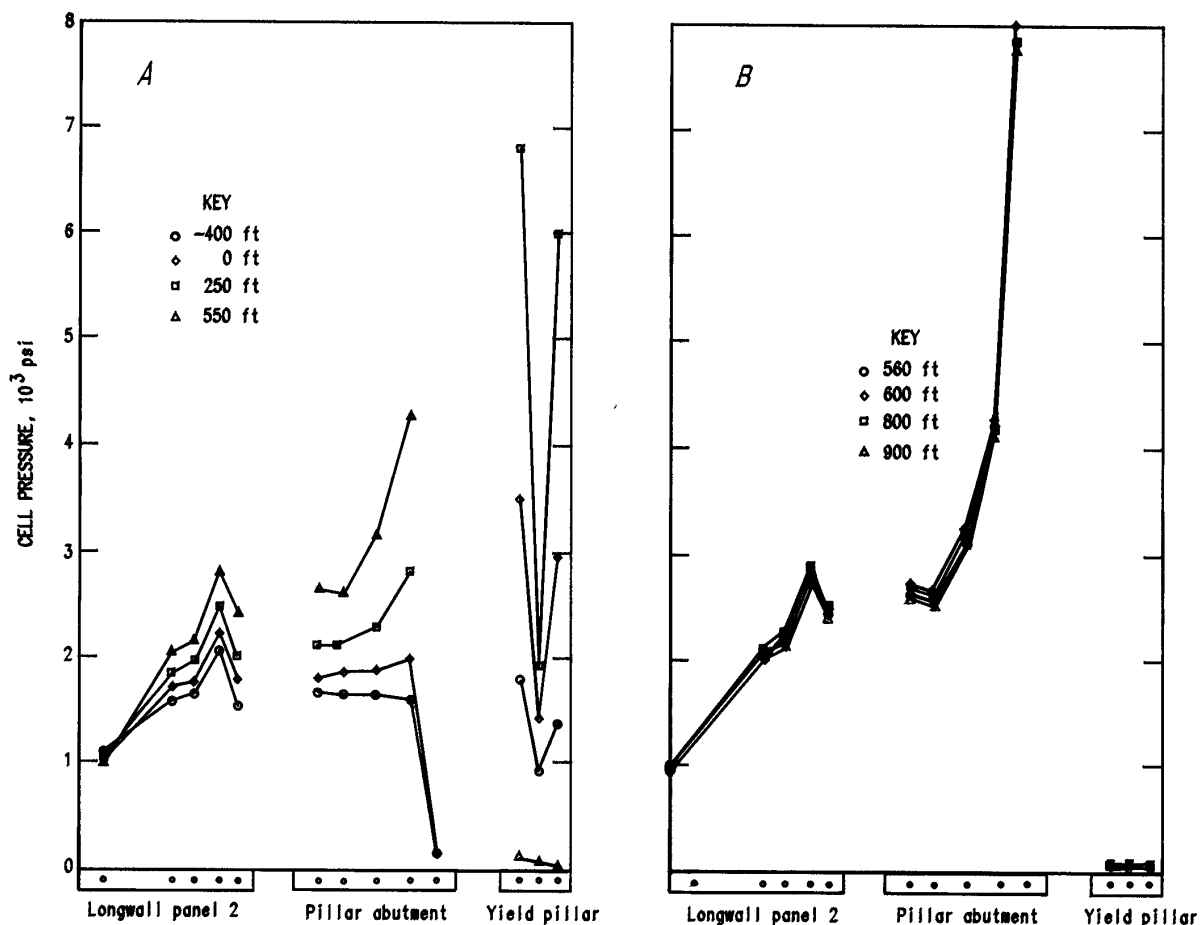


Figure 23.—Stress profiles at headgate site B. A, Face distances from -400 ft (face inby) to 500 ft (face outby); B, outby face distances to 1,000 ft.

The site H pressure profiles (fig. 22) indicate that maximum yield pillar loading occurred at approximately the same face distance (350 ft) that cavity collapse occurred. This maximum loading may indicate the distance at which side-abutment effects extend behind the face. Postfailure pressure profiles suggest that the abutment pillar and panel 2 tailgate rib experienced stress increases because of yielding of the small chain pillar (fig. 22). Passage of the face from 400 to 1,000 ft resulted in small increases on the panel 2 rib, but significant pressure increases on the abutment pillar. Abutment pillar increases apparently resulted from continued yielding of the small chain pillar and stress redistributions, resulting from yielding of the abutment pillar rib (fig. 22). Included in the panel 2 study is a gob reloading site. While this preliminary analysis suggests that side-abutment effects extend

to about 350 to 400 ft behind the face and that pillar yielding increases stress on the abutment pillar and on the panel 2 tailgate rib, firm conclusions regarding pillar stress changes and load transfers between the pillars and the gob will have to await the panel 2 gob pressure results.

In summary, the load transfer analysis suggests that (1) maximum stress levels and main roof caving occur "simultaneously;" (2) this distance represents the side-abutment extent; (3) small chain pillar yielding causes stress buildups on both the abutment pillar and panel 2 tailgate; (4) the tailgate rib is under increased stress because of panel 1 mining and maximum pressure increases occur at 10 to 20 ft inside the rib; and (5) the abutment pillar and tailgate rib were highly stressed for panel 2 mining.

A comparison between the longwall-induced pressures on the two-entry configurations, a tailgate supported by

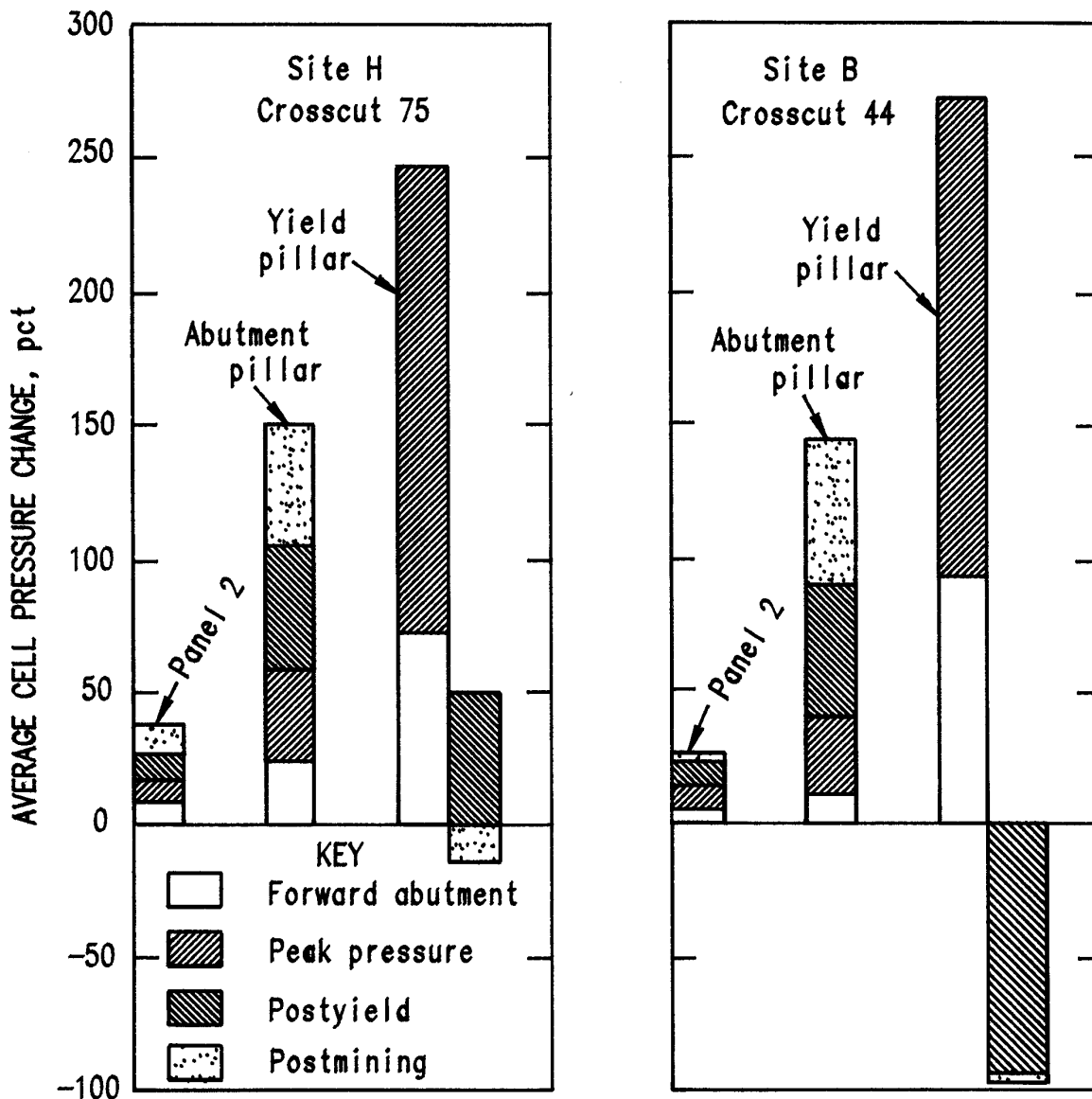


Figure 24.—Mean pressure increases at headgate sites H and B. A, Face distances from -400 ft (face inby) to 500 ft (face outby); B, outby face distances to 900 ft.

two rigid pillars, and a headgate with both a rigid and yielding chain pillar is shown in figures 25 and 26. Both the headgate and tailgate entry systems were instrumented prior to longwall mining, and the tailgate entries were not subjected to any previous longwall mining influence.

Panel 1 mining induced significant loading on the tailgate rib of panel 2, but did not transfer significant load onto the solid coal adjacent to the panel 1 tailgate chain

pillars. The tailgate chain pillars responded elastically and essentially isolated any panel 2 mining influence. The headgate abutment pillar pressures exceeded those measured in the tailgate. Higher pillar pressures were attributed to elastic stress increases because of being closer to panel 1 than its panel 2 counterpart and stress transfer resulting from yielding of the small, adjacent chain pillar (I).

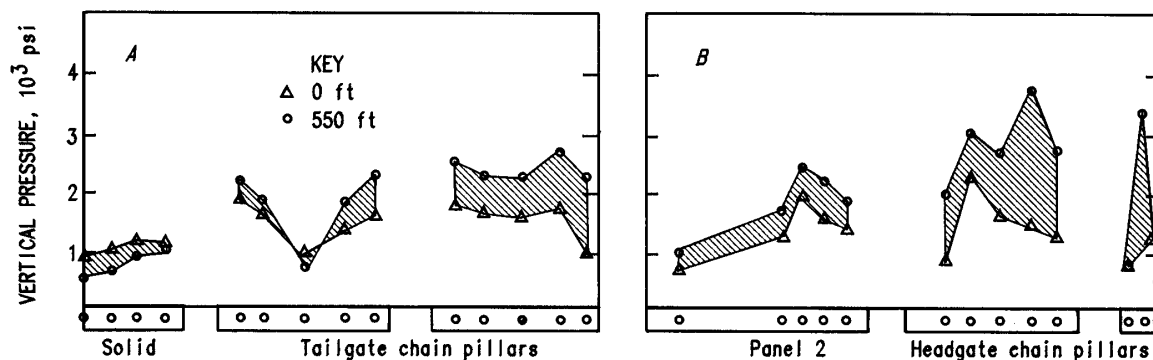


Figure 25.—Panel 1 mining effect on tailgate and headgate pressure distribution at sites T (A) and H (B).

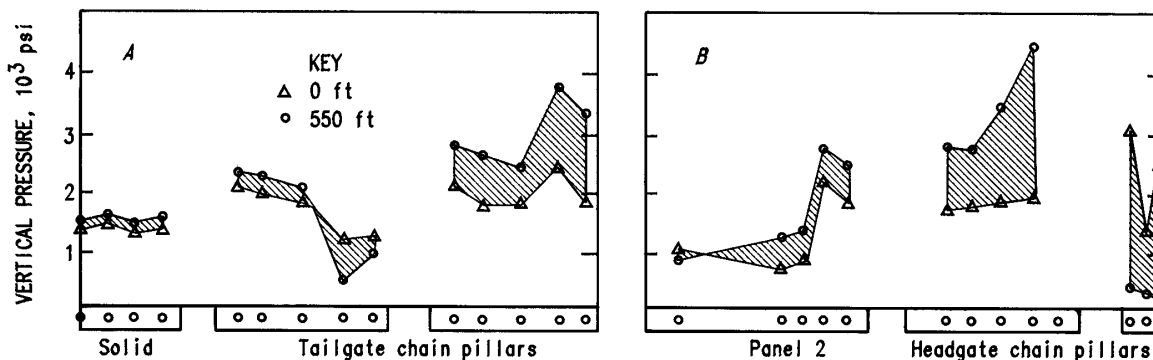


Figure 26.—Panel 1 mining effect on tailgate and headgate pressure distribution at sites A (A) and B (B).

SUMMARY AND CONCLUSIONS

This study provided a unique opportunity to assess large-scale strata response to first panel longwall mining. As the instrumentation sites were designed to measure large-scale behavior, detailed analysis of pillar stresses, intersection stability, and immediate roof behavior were not performed. Panel 2 mining past the most recently installed sites, one including a gob reloading station and the other in the fault area, should improve understanding of any roof action-load transfer mechanisms and determine whether the present abutment pillar size functions as designed. Results of this study suggest that the large-scale strata response at this mine is controlled by a relatively shallow overburden with good caving characteristics, and a strong coal with a well-defined face cleat.

Pressure measurements generally agreed with previous western U.S. coal mine observations that forward abutment effects begin at a distance about one-quarter to one-third the depth ahead of the face, and that significant increases begin when the face is about 0.1 ft depth away. Unlike other studies, however, no evidence exists for a significant yield zone at the face. The shallow overburden (1,050 ft) and good caving characteristics of the main roof apparently do not generate the stresses necessary to cause significant yielding of the coal face. Another possible contributing factor is the high face retreat rate (40 to 60 ft per day) that minimized any time-dependent loading.

Yield pillar studies determined that the present pillar width did not function as designed; panel 1 mining induced yielding, but not until the face retreated outby. Mixed evidence suggested that the yield pillars are near critical width, contained a stressed core that later stabilized, yielded without observed bumping, and the widths could be reduced if the immediate roof can withstand additional deflection. Two yield pillar design techniques indicated that in-mine behavior could be simulated. However, these methods are very sensitive to material properties,

and it is suggested that "fine tuning" a yield pillar size should include, if possible, site-specific measurements and properties.

Entry system pressure redistribution (load transfer) resulted from the panel 1 side-abutment loading and small chain pillar yielding. Maximum yield pillar loading occurred at approximately the outby face distance at which the main roof cavity collapsed. Subsequent failure of the yield pillar increased pressure on the abutment pillar and panel 2 tailgate rib, especially up to 20 ft within the rib. Continued loading of the panel 2 tailgate rib and adjacent abutment pillar apparently resulted from continued small pillar yielding and observed yielding of the abutment pillar rib closest to panel 1.

Panel 2 conditions are difficult to predict, but the results indicate some potential areas of concern. Panel 2 tailgate stresses, especially within 20 ft of the rib, may contribute to face bump severity. The abutment pillar is highly stressed, and second panel mining could increase the likelihood of pillar bumping. Actual conditions will dictate the final pillar sizes, but this analysis indicates that the present headgate design is adequate for first panel mining. This study did not include a detailed roof behavior site, and it may be that the final entry design will depend on maximizing the stability of the lower 10 ft of slickensided, easily fractured immediate roof. Narrower pillar widths have the advantages of earlier stress transfers and potentially lower tailgate stresses if the transferred stresses are sufficient to induce panel 2 tailgate rib yielding. The disadvantages include larger stress transfers onto the panel 2 tailgate if yielding of this rib does not occur and, possibly, increased roof problems due to increased deflection. Wider pillars should reduce load transfer onto the tailgate rib, but they create higher stress zones on the pillar edges and could contribute to roof or rib failures, especially at the pillar corners.

REFERENCES

1. Hanna, K., K. Y. Haramy, and T. Ritzel. Automated Longwall Mining for Improved Health Safety and Productivity at the Foidel Creek Mine. Soc. Min. Eng. AIME preprint 91-165, 1991, 8 pp.
2. Conover, D. P., K. Hanna, and T. L. Muldoon. Mine-Wide Monitoring Applications in Ground Control Research. Paper in Proceedings of the Ninth International Conference on Ground Control in Mining, ed. by S. S. Peng (June 4-7, 1990). Dep. Min. Eng., Coll. Miner. and Energy Resour., WV Univ., Morgantown, WV, 1990, pp. 135-141.
3. Haramy, K. Y., W. C. Smith, and R. O. Kneisley. Automated Ground Control Monitoring. Paper in Proceedings of the Third Conference on Ground Control Problems in the Illinois Coal Basin, ed. by Y. P. Chugh (Aug. 8-10, 1990). Dep. Min. Eng., South IL Univ., Carbondale, IL, 1990, pp. 227-235.
4. Maleki, H., M. Hardy, and R. Tiftt. Geomechanical Mine Design of the Foidel Creek Mine. Paper in Proceedings of the Seventh International Conference on Ground Control in Mining, ed. by S. S. Peng (Aug. 3-5, 1988). Dep. Min. Eng., Coll. Miner. and Energy Resour., WV Univ., Morgantown, WV, 1988, pp. 137-148.
5. Bickel, D. L., and D. A. Donato. In Situ Horizontal Stress Determinations in the Yampa Coalfield, Northwestern Colorado. Bu-Mines RI 9149, 1988, 43 pp.

6. Dowding, C. H., M. B. Su, and K. M. O'Connor. Measurement of Rock Mass Deformation With Grouted Coaxial Antenna Cables. *Rock Mech. and Rock Eng.*, v. 22, No. 1, 1989, pp. 1-23.
7. O'Connor, K. M., and T. Zimmerly. Application of Time Domain Reflectometry to Ground Control in Potash Mining. Paper in Proceedings of Tenth International Conference on Ground Control in Mining, ed. by S. S. Peng (June 10-12, 1991). *Dep. Min. Eng., Coll. Miner. and Energy Resour., WV Univ., Morgantown, WV*, 1991, pp. 115-121.
8. Haramy, K. Y., and R. O. Kneisley. Comparative Study of Western U.S. Longwall Panel Entry Systems. Paper in Proceedings of 30th U.S. Rock Mechanics Symposium, ed. by A. W. Khair (June 19-22, 1989). *Balkema*, 1989, pp. 125-132.
9. DeMarco, M. J., J. R. Koehler, and P. H. Lu. Characterization of Chain Pillar Stability in a Deep Western Coal Mine—Case Study. *Soc. Min. Eng. AIME preprint 88-76*, 1988, 11 pp.
10. Haramy, K. Y., R. O. Kneisley, and J. P. McDonnell. Longwall Face Bursts and Inadequate Caving: A Case Study. Paper in Proceedings of Sixth International Conference on Ground Control in Mining, ed. by S. S. Peng (June 9-11, 1987). *Dep. Min. Eng., Coll. Miner. and Energy Resour., WV Univ., Morgantown, WV*, 1987, pp. 18-31.
11. Haramy, K. Y., and R. O. Kneisley. Yield Pillars for Stress Control in Longwall Mines. *Int. J. Min. and Geol. Eng.*, v. 8, 1990, pp. 287-304.
12. Lu, P. H. Mining-Induced Stress Measurements with Hydraulic Borehole Pressure Cells. Paper in Proceedings of Twenty-Fifth Symposium on Rock Mechanics (Northwestern Univ., Evanston, IL, June 25-27, 1984). *Soc. Min. Eng. AIME*, Littleton, CO, 1984, pp. 204-211.
13. _____. A New Method of Rock Stress Measurement With Hydraulic Borehole Pressure Cells. Paper in Proceedings of International Symposium on Rock Stress and Rock Stress Measurements, Stockholm, Sweden (Sept. 1-3, 1986). *CENTEK Publ., Lulea, Sweden*, 1986, pp. 237-245.
14. Wilson, A. H. Research Into the Determination of Pillar Size: An Hypothesis Concerning Pillar Stability. *Min. Eng. (London)*, v. 131, 1972, pp. 409-417.
15. _____. The Stability of Underground Workings in the Soft Rocks of the Coal Measures. Ph.D. Thesis, *Univ. Nottingham, United Kingdom*, 1980, 204 pp.
16. Karmis, M., and G. Chen. An Investigation Into Yield Pillar Behavior and Design Considerations. Paper in Proceedings of the Multinational Conference on Mine Planning and Design, ed. by G. T. Lineberry and K. F. Unrug (May 23-26, 1989). *Univ. KY, Lexington, KY*, 1989, pp. 13-20.
17. Chen, G., and M. Karmis. Computer Modeling of Yield Pillar Behavior Using Post-Failure Criteria. Paper in Proceedings of the Seventh International Conference on Ground Control in Mining, ed. by S. S. Peng (Aug. 3-5, 1988). *Dep. Min. Eng., Coll. Miner. and Energy Resour., WV Univ., Morgantown, WV*, 1988, pp. 116-125.